Atmos. Chem. Phys. Discuss., 9, 22459–22504, 2009
www.atmos-chem-phys-discuss.net/9/22459/2009/

Atmospheric Chemistry and Physics Discussions

This discussion paper is/has been under review for the journal *Atmospheric Chemistry and Physics (ACP)*. Please refer to the corresponding final paper in *ACP* if available.

Impact of energetic particle precipitation on stratospheric polar constituents: an assessment using MIPAS data monitoring and assimilation

A. Robichaud[1], R. Ménard[1], S. Chabrillat[2], J. de Grandpré[1], Y. J. Rochon[3], Y. Yang[3], and C. Charette[1]

[1]Atmospheric Science and Technology Directorate, Environment Canada, 2121 Trans-Canada Highway, Dorval (Québec), H9P 1J3, Canada
[2]Belgium Institute for Space Aeronomy Avenue Circulaire 3, 1180, Bruxelles, Belgium
[3]Atmospheric Science and Technology Directorate, Environment Canada, 4905 Dufferin Street, Toronto (Ontario), M3H 5T4, Canada

Received: 23 September 2009 – Accepted: 2 October 2009 – Published: 23 October 2009

Correspondence to: A. Robichaud (alain.robichaud@ec.gc.ca)

Published by Copernicus Publications on behalf of the European Geosciences Union.

Abstract

In 2003, strong geomagnetic events occurred which produced massive amounts of energetic particles penetrating the top of the atmospheric polar region, significantly perturbing its chemical state down to the middle stratosphere. These events and their effects are generally left unaccounted for in current models of stratospheric chemistry and large differences between observations and models are then noted. In this study, we use a coupled 3-D stratospheric dynamical-chemical model and assimilation system to ingest MIPAS temperature and chemical observations. The goal is to gain further understanding and to evaluate the impacts of EPP (energetic particle precipitation) on stratospheric polar chemistry. Moreover, we investigate the feasibility of assimilating valid "outlier" observations associated with such events. We focus our analysis on *OmF* (Observation minus Forecast) residuals as they filter out phenomena well reproduced by the model (such as gas phase chemistry, transport, diurnal and seasonal cycles) thus revealing a clear trace of the EPP. Inspection of *OmF* statistics in both the passive (without chemical assimilation) and active (with chemical assimilation) cases altogether provides a powerful diagnostic tool to assess the model and assimilation system. We also show that passive *OmF* can permit a satisfactory evaluation of the ozone partial column loss due to EPP effects. Results suggest a small but significant loss of 5–6 DU (Dobson Units) during an EPP-IE (EPP indirect effects) event in the Antarctic winter of 2003, and about only 1 DU for the SPE (solar proton event) of October/November 2003. Despite large differences between the model and MIPAS chemical observations (NO_2, HNO_3, CH_4 and O_3), we demonstrate that a careful assimilation of these constituents with only gas phase chemistry included in the model (i.e. no provision for EPP impacts) and with relaxed quality control nearly eliminated the short-term bias and significantly reduced the standard deviation error below 1 hPa.

ACPD

9, 22459–22504, 2009

1 Introduction

It has been known for a long time that the main source of global stratospheric NO_x is the oxidation of N_2O from the troposphere. However, energetic particle precipitation (EPP) is considered as the most important secondary source. These particles are either high energetic electrons or protons that can produce NO directly in the stratosphere if their energies are respectively greater than 300 keV and 30 MeV (Randall et al., 2006). EPP, solar and galactic cosmic rays which penetrate into the polar middle atmosphere at high latitudes give rise to ionization, dissociation, dissociative ionization and excitation processes (Brasseur and Solomon, 2005; Jackman et al., 2008). EPP exerts a larger influence on polar ozone on a decadal scale than previously thought (Sinnhuber et al., 2006). On short to medium time scales, EPP influences the production of odd hydrogen (HO_x) and odd nitrogen (NO_y) which can affect ozone chemistry through chemical catalytic cycles (Solomon and Crutzen, 1981; Brasseur and Solomon, 2005; Turunen et al., 2009). The high values of NO_x (NO, NO_2) and HO_x (H, OH, HO_2) produced by EPP, which can descend in the mesosphere and upper stratosphere at polar latitudes (>60°) of both hemispheres, have been the subject of many controversies, particularly in the way they affect the ozone budget. Significant photochemical loss has been reported by many authors in the upper stratosphere associated with these disturbances (Callis et al., 1996; Jackman and McPeters, 2004; Rozanov et al., 2005; Seppälä et al., 2007; WMO, 2007). For example, during a very strong solar proton event in July 2000, measurements from the UARS HALOE and NOAA 14 SBUV/2 instruments indicated short-term (time scale of a day) middle mesospheric ozone decreases of over 70% caused by short-lived HO_x during the event with a medium-term (several days) upper stratospheric ozone depletion of up to 9% caused by longer-lived NO_x (Jackman et al., 2001). With the use of a 3-D numerical model, Rozanov et al. (2005) showed that atmospheric chemistry throughout the whole atmosphere down to the surface is significantly perturbed by EPP indirect effects (thereafter referred to as EPP-IE following Randall et al., 2006). EPP-IE in this case is linked with ionized particles trapped in the

ACPD
9, 22459–22504, 2009

magnetosphere which precipitate into the upper atmosphere ejected by the solar wind or solar disturbances.

Evidence of high amounts of upper stratospheric and mesospheric polar NO_2 and anomalous values of HNO_3 as measured by the MIPAS/ENVISAT mission (Fischer and Oelhaf, 1996; Fischer et al., 2007; ESA, 2000) have been documented in the recent literature (Funke et al., 2005; Stiller et al., 2005; Orsolini, 2005). Anomalous but continuous downward transport of these chemical constituents from the mesosphere and lower thermosphere (MLT) region into the upper stratosphere starting from the end of May and extending to September 2003 was found to be linked to several geomagnetic and EPP-IE events occurring in a rather continuous fashion in the MLT (Stiller et al., 2005; Funke et al., 2005). On the other hand, a more spectacular event such as a SPE (solar proton event) had also occurred the same year towards to end of October 2003 (referred as the "Halloween storm"; see Baker et al., 2004). SPEs which are rather sporadic in nature occur more frequently near the solar maximum or during its declining phase. They have recently been widely documented both with sophisticated models (Jackman et al., 2008 and references therein; Semeniuk et al., 2005) and in observational studies (Lopez-Puertas, 2005; Orsolini et al., 2005). SPEs are specifically linked with solar flares and/or coronal mass ejections. Both types of EPP (EPP-IE and SPE) could be modulated by meteorological conditions influencing the downward transport of chemical constituents to the stratosphere (Randall et al., 2006, 2007; Siskind et al., 2007). The rate of descent at high latitudes is linked to the strength of the polar vortex (Manney et al., 1994; Seppälä et al., 2004) and possibly enhanced at times by a complex combination of dynamical factors and coupling between the stratosphere and the mesosphere as discussed in Siskind et al. (2007). Accompanying the high NO_x are anomalously high HNO_3 values in the polar stratosphere (Orsolini et al., 2005) which could be explained by ion cluster chemistry reactions (Kawa, 1995) and/or by heterogeneous reactions of NO_x on sulphate aerosols via N_2O_5 or, less likely, by simple gas phase reactions (see Stiller et al., 2005 for a discussion). HO_x and NO_x gases have a short chemical lifetime since they are mainly destroyed by photo-dissociation. But

during the polar winter, when little or no sunlight is available, the impacts of NO_x can survive longer and even extend outside the polar region through downward transport processes across the stratopause, thus affecting more significantly the total ozone column.

In our study, we use a new comprehensive coupled stratospheric chemistry-meteorology 3-D global model called GEM-BACH (Ménard et al., 2007; hereafter M2007) together with MIPAS observations. We calculate the mean and standard deviation of passive (without chemical assimilation) versus active (with chemical assimilation) *OmF* (observation minus forecast) residuals of long-lived species (O_3, NO_2, HNO_3 and CH_4) during the second half of 2003. EPP events are not physically accounted for in our model but we demonstrate that the signature of these tracers can be correctly identified by passive *OmF* plots in observation space as shown in Sect. 5 when downward transport of excess NO_y or HO_x occurs. Throughout this study, a comparison is also made with the case that includes chemical assimilation (active *OmF*). Together, these sets of cross sections (passive and active *OmF*s) constitute an excellent diagnostic and monitoring tool for model-assimilation systems. They help to track the signature of EPP and other related phenomena (such as heterogeneous ion-cluster chemistry) which are not taken into account in most stratospheric models. In Sect. 3 we provide a theoretical derivation explaining the conditions of success of assimilation in the presence of important model chemical biases. The methods and diagnostics are described in Sect. 4 and the results and applications in Sect. 5. An evaluation of ozone loss due to the EPP during the second half of 2003 is also performed using *OmF* diagnostics. Finally, Sect. 6 presents a summary and the conclusions.

ACPD

9, 22459–22504, 2009

2 GEM-BACH model, data assimilation system and observations

2.1 Model

We use the model GEM-BACH v3.3.0 (Global Environmental Multi-scale coupled with the Belgium Atmospheric CHemistry), which has emerged from a collaboration between Canada and Belgium. It is a comprehensive 3-D global chemistry circulation model (GCCM) based on the stratospheric version of the Canadian NWP model called GEM (Côté et al., 1998) and the stratospheric chemistry developed for BASCOE (Errera and Fonteyn, 2001). The coupled model allows chemistry-radiative feedbacks (M2007; de Grandpré et al., 2009). The model has 80 vertical levels, including 27 in the stratosphere, and is integrated at a horizontal resolution of 1.5° by 1.5° (a grid of 240 by 120) with a lid at 0.1 hPa, allowing stratospheric channels of TOVS (AMSU-A channels 9–14) and MIPAS observations (mostly stratospheric) to be assimilated. The vertical resolution of the model ranges from 0.5 to 3 km in the stratosphere (with ∼1.5 km at 30 km) and 3–4 km in the lower mesosphere, with a higher resolution in the troposphere. Semi-implicit and semi-Lagrangian numerical techniques optimized to handle a large number of advection equations for the transport of species are utilized by the model (a more complete description is available in M2007). On the other hand, an on-line coupled comprehensive stratospheric chemistry module developed at the Belgium Institute of Aeronomy (Errera and Fonteyn, 2001) has been implemented in our framework. It includes 57 species which interact through 143 gas-phase reactions, 48 photolysis reactions and 9 heterogeneous reactions. The chemistry package is built with the Kinetic Preprocessor (Damian et al., 2002) and the scheme is integrated using a third order Rosenbrock solver (Hairer and Wanner, 1996). The chemical and photo-dissociation rates follow the Jet Propulsion Laboratory compilation by Sander et al. (2003). The heterogeneous chemistry is parameterized as a simple function of temperature and a prescribed climatology for sulfate area densities. Polar Stratospheric Clouds (PSC) are formed when temperatures are below 194 K (NAT particles) or 186 K (ice particles). This photochemical module was used operationally

ACPD
9, 22459–22504, 2009

in BASCOE and has been fully validated (see M2007). Only gas phase and heterogeneous chemistry are represented in our model. Therefore, no provisions for ion, ion production/recombination, ion-neutral coupling or ion-cluster chemistry exist in our framework which would be required in principle to fully simulate EPP effects.

2.2 Assimilation system

The assimilation algorithm is a variational 3D-VAR 6-h cycle (Gauthier et al., 1999) with calculation of *OmF* (observation minus forecast) using the model forecasts at the time steps nearest to the observation times, i.e. FGAT (First Guess at Appropriate Time). The latter approach was selected since it permits a better time resolution than that of the standard 3D-VAR, which is crucial for fast time scale assimilated constituents such as NO_2 in the middle atmosphere (M2007). Error statistics needed for the assimilation algorithm have been built using the NMC method (Parrish and Derber, 1992) for the dynamics. The method of H-L (Hollingsworth and Lönnberg, 1986) adapted for satellite measurements (see M2007) was applied in setting the constituent error variances. The error correlations for constituents were estimated from 6-h time differences of fields from a standard model run (Polavarapu et al., 2005). The set of operational MIPAS chemical constituents and temperature observations presented to the minimization algorithm is obtained after filtering outliers using the quality check applied operationally at CMC (Canadian Meteorological Center), which rejects data whenever *OmF* residuals are greater than 5 times the estimated *OmF* standard deviations. This is considered as a relaxed gross error check as compared to the value of 3 traditionally used (Gauthier et al., 2003). Special treatment of the assimilation error statistics has to be applied so that the observed high values of NO_y produced by EPP do not get filtered out by the quality control such as in Errera et al. (2008). The resulting transport and dynamics in our system has been verified in M2007 with independent data and found to be very reliable in both the troposphere and stratosphere in situations with and without EPP effects.

ACPD
9, 22459–22504, 2009

2.3 MIPAS/ENVISAT observations

The MIPAS (Michelson Interferometer for Passive Atmospheric Sounding) instrument was launched on 1 March 2002 onboard ESA's ENVISAT (European Space Agency ENVironmental SATellite), which is a sun-synchronous polar-orbiting satellite flying at about 800 km altitude with a 98.55° inclination. MIPAS provides day and night time measurements from pole to pole, which allows observation of the Arctic and the Antarctic areas during the polar vortex season. In particular, the simultaneous observation of HNO_3 and NO_2 in the polar night makes possible the assessment of chemical transformation within the NO_y family occurring during EPP events. The MIPAS instrument is a slow downward limb scanning Fourier spectrometer, which measures the complete spectrum of limb emission in the frequency interval 680–2410 cm^{-1} of the mid-infrared spectrum (corresponding to the wavelength range of 4.1–14.5 μm). A spectrum is acquired every 4.6 s at each of the 17 tangent altitudes giving about 1000 profiles per day, starting at an altitude of 68 km down to 6 km. The average number of orbits is 14.4 per day. The field of view at the tangent heights is ~3 km by 30 km with a resolution of 500 km along track and about 2800 km across track at the Equator. The vertical resolution is about 3 km in the stratosphere but lower in the mesosphere (Fischer et al., 2007).

The retrieved profiles for this study have been obtained by non-linear least square fitting using the Optimized Retrieval Model (ORM), which has the advantage of maximum vertical resolution but has the disadvantage of the possibility of oscillatory profiles. The main challenge of the ORM has been the requirement of performing the complex operation of mathematical inversion in near real time for a large number of data (Fischer et al., 2007). Other options exist, such as more accurate retrievals performed by IMK [1] using Tikhonov regularization, which is more stable than ORM (von Clarmann, 2007). However, MIPAS-IMK retrieval products are not available for all measurement days, as opposed to the MIPAS-ESA products.

[1] IMK: Institut für Meteorologie und Klimaforschung, at Karlsruhe, Germany

ACPD
9, 22459–22504, 2009

In the stratosphere, comparing MIPAS observations (version 4.61 of MIPAS-ESA retrieval profiles in near-real time) to HALOE (V 19) gives biases of −1 to +3 K between the two instruments. In the lower stratosphere, the biases are a little less, that is about 0.5 to 2.5 K (Dethof et al., 2004). Wang et al. (2005) reported that mean differences with other sources are within 0.5 K as averages and within 1–1.5 K at individual levels between 10–30 km. Typical r.m.s errors for ozone were found to be in the range 5–15% (Dethof et al., 2003; M2007) and for H_2O, CH_4, N_2O and NO_2, around 25–35% (Baier et al., 2005; M2007). Note that, in general, MIPAS-ESA errors in the stratosphere are also acceptable for NO_2. However, according to Funke et al. (2005), NO_2 from MIPAS-ESA retrievals is underestimated by 30% above 50 km, mostly due to physical processes not taken into account by MIPAS-ESA retrievals such as non-LTE (non local thermodynamic equilibrium) processes.

The period under study is the second half of 2003 due to the near continuous day to day availability of MIPAS-ESA data during this time. It also happens that 2003 is considered a very active year from the geomagnetic point of view (http:/www.spwc.noaa.gov). The assimilation period extends from the second week of August to the first week of December 2003. Note that in the Northern Hemisphere, the polar vortex had shrunk in the second half of December (after the end of our analyzed period) due to a sudden warming episode, producing a distortion of the EPP signal.

3 Data assimilation in presence of chemical model biases

Assimilation schemes generally assume that both model and observations have no systematic errors or biases. However, for a number of reasons, the model may have inadequate or missing representation of some physical processes which can give rise to significant model biases. The presence of model biases (caused by EPP impacts for example) can be detected in the mean observation-minus-forecast residuals. The assimilation of meteorological observations will not eliminate model biases from the analysis and forecasts no matter how the observation and background error statistics

ACPD
9, 22459–22504, 2009

are prescribed, unless an additional step is introduced in the assimilation scheme, known as the bias correction (see Dee and daSilva, 1998, or Ménard, 2009 and references therein for further details). In the case of temperature assimilation, a bias correction based on MIPAS temperature using standard procedures has been applied to AMSU-A observations before assimilation (see M2007 for more details). But for chemical constituents no such correction scheme is utilized in this study. We rather argue that careful assimilation of chemical constituents could correct the bias under the circumstances discussed below. As an illustrative example, consider a persistence model for chemical concentrations. Suppose that the reality represented here by the true state $\boldsymbol{x}^t$ is governed by the following equation,

$$\boldsymbol{x}^t_{n+1} = \boldsymbol{x}^t_n + \boldsymbol{q}\Delta t, \tag{1}$$

where n is the time step and q is the net production rate that is not included in the atmospheric chemistry model (such as caused by EPP impacts) but present in the atmosphere and Δt, the time scale. In this context of a model based on persistence, a forecast $\boldsymbol{x}^f_{n+1}$ at time t_{n+1} issued from an analysis $\boldsymbol{x}^a_n$ at time t_n takes the simple form

$$\boldsymbol{x}^f_{n+1} = \boldsymbol{x}^a_n. \tag{2}$$

The forecast and analysis error defined as $\boldsymbol{\varepsilon}^f = \boldsymbol{x}^f - \boldsymbol{x}^t$, $\boldsymbol{\varepsilon}^a = \boldsymbol{x}^a - \boldsymbol{x}^t$ are then related by equation

$$\boldsymbol{\varepsilon}^f_{n+1} = \boldsymbol{\varepsilon}^a_n - \boldsymbol{q}\Delta t. \tag{3}$$

The mean error or bias is then also governed by the equation,

$$\bar{\boldsymbol{\varepsilon}}^f_{n+1} = \bar{\boldsymbol{\varepsilon}}^a_n - \boldsymbol{q}\Delta t, \tag{4}$$

since $\boldsymbol{q}$ is a deterministic quantity. In general, 3D-VAR (but also Kalman filters and Optimum Interpolation) have the following (unbiased) form (Kalnay, 2003)

$$\boldsymbol{x}^a_n = \boldsymbol{x}^f_n + \mathbf{K}(\boldsymbol{y}^o_n - \mathbf{H}\boldsymbol{x}^f_n) \tag{5}$$

ACPD
9, 22459–22504, 2009

where **K** is the Kalman gain matrix, **H** is the observation operator (which includes interpolation for the observations location to the discrete model representation, and $\boldsymbol{y}_n^o$ is the observation vector. Assuming that the observations

$$\boldsymbol{y}_n^o = \mathbf{H}\boldsymbol{x}_n^t + \boldsymbol{\varepsilon}_n^o, \tag{6}$$

are unbiased, i.e. $\bar{\boldsymbol{\varepsilon}}_n^o = 0$ and subtracting $\boldsymbol{x}_n^t$ from (Eq. 5), leads to

$$\bar{\boldsymbol{\varepsilon}}_n^a = (\mathbf{I} - \mathbf{KH})\bar{\boldsymbol{\varepsilon}}_n^f. \tag{7}$$

Note that (**I**−**KH**) represents the reduction of variance (covariance) due to the assimilation of observations. In a scalar case and in a simplified context of having observations at each grid point, the reduction of variance, that we denote by m, is simply

$$m = I - KH = \frac{\sigma_o^2}{\sigma_f^2 + \sigma_o^2}, \tag{8}$$

where σ_f^2 and σ_o^2 denote respectively the forecast and observation error variances. The following constraint applies on m

$$0 < m < 1. \tag{9}$$

Combining the scalar form of Eqs. (4) and (7) gives an evolution equation for the forecast error bias of the form,

$$\bar{\varepsilon}_{n+1}^f = -q\Delta t + (I - KH)\bar{\varepsilon}_n^f. \tag{10}$$

In the simplified scalar case above, i.e. Eq. (8), we have

$$\bar{\varepsilon}_{n+1}^f = -q\Delta t + m\bar{\varepsilon}_n^f, \tag{11}$$

from which a simple solution can be found, i.e.

$$\bar{\varepsilon}_n^f = m^n\bar{\varepsilon}_0^f - q(1 + m + m^2 + \ldots + m^{n-1})\Delta t = m^n\bar{\varepsilon}_0^f - q\frac{(1-m^n)}{(1-m)}\Delta t. \tag{12}$$

ACPD
9, 22459–22504, 2009

Since $m<1$ the asymptotic solution for large n is readily obtained as

$$\bar{\varepsilon}^f_\infty \rightarrow -\frac{q}{1-m}\Delta t, \tag{13}$$

and the mean observation-minus-forecast residuals (OmF) converges to

$$(\overline{OmF})_\infty \rightarrow \frac{q}{1-m}\Delta t. \tag{14}$$

Note that the bias in the initial conditions ($\bar{\varepsilon}^f_0$) is eliminated as n becomes large (see Eq. 12). There are associated time scales in Eqs. (13) and (14) that are important to consider for the interpretation of this result. In this derivation, the time scale is tied to the assimilation cycle, but more precisely to the revisit time of the satellite over the same region so that, in effect, a reduction of variance is accounted for with m or $(I-KH)$. For ENVISAT, the revisit time is Δt=12 h and the production rate q should thus be measured with respect to this time scale. For example, suppose that the production rate q is slow, taking say 30 days to double the initial concentration x_0, i.e. $q \approx x_0/(60\Delta t)$. On the other hand, it is often the case that the observation error variance and the forecast error variance are not that different in value so that $1-m \approx 1/2$. In this case, we obtain from Eq. (14), $\overline{OmF} \approx x_{0/30}$.The model bias and the mean observation-minus-forecast residual are, with this simple calculation, of the order of 3%, whereas observation and forecast error standard deviation are usually somewhat larger, typically 10–20%. The mean observation-minus-forecast residual is in this case smaller than the standard deviation of the OmF and successful assimilation is expected despite large initial biases. At the other extreme, where the production rate is fast, say on the order of a day, we have $\overline{OmF} \approx x_0$, and the mean OmF (~100%) then far exceeds its standard deviation likely leading to unsuccessful assimilation. Although the full analysis would entail the computation of $(I-KH)$ which is beyond the scope of this paper, this simple analysis is nevertheless useful in providing a qualitative interpretation and a deeper understanding of the results presented in the following sections.

4 Description of methods and diagnostics

We define here two kinds of observation-minus-co-located forecast (*OmF*) differences: 1 – offline (or "passive") where the chemical observations are not used to initialize the model forecasts, and 2 – online (or "active") where, through the use of an assimilation system, the observations are ingested and serve to initialize the short-term forecasts. *OmF* in the latter differences are also referred to as *innovations* (Daley, 1991).

In the offline mode, excess concentrations of constituents due to EPP effects can be isolated by taking the differences between chemical observations and co-located chemical forecasts driven by assimilated temperature and wind measurements. Taking these differences (*OmF*) actually filters out the effects of transport, gas phase chemistry, diurnal, seasonal, annual and semi-annual cycles which are generally well reproduced by our model, and thus allows isolation of the chemical anomalies caused by EPP. Furthermore, since EPP produces strong excesses of chemical constituents of the NO_y and HO_x families (e.g. NO_2, HNO_3, OH, HO_2, etc.) which are not represented in our model, the observation-minus-forecast differences (i.e. the *OmF*s) have magnitudes well above the observation errors or chemical transport modeling uncertainties, and thus truly represent EPP effects. Tracking the daily zonal mean and standard deviation of *OmF* as a function of time and height provides a powerful diagnostic and analysis tool of the EPP effects – a novel approach used in this study.

On the other hand, the impact of assimilating observations is generally seen through a reduction of the mean and standard deviations of the *OmF* from offline to online. For instance, in situations where the initial conditions are grossly in error but the model has no bias, very large mean offline *OmF* are to be expected. The *OmF* can likewise be reduced significantly from offline to online only if the model bias growth rate time scale is much longer than the observation revisit time. However, if the growth rate time scale is comparable to the observations revisit time scale, a significant reduction of the *OmF* from offline to online cannot be achieved, as was argued in Sect. 3. The behavior of *OmF*s from offline to online thus turns out to be a useful diagnostic for the

ACPD
9, 22459–22504, 2009

presence and time scale of the model biases. It also reflects the quality of the assimilation process. For example, large mean values of passive *OmF* biases (i.e. without chemical assimilation) caused by EPP which are eliminated in the active *OmF* biases system (i.e. with chemical assimilation) denote either: 1) errors in the initial conditions or 2) systematic model bias linked to slow time scale (a few weeks to a few months) chemical processes. In our study, these errors mostly originate due to the absence of proper EPP modeling. Fast time scale errors will not be corrected by assimilation as discussed in Sect. 3. Note that intermittent physical phenomena such as EPP impacts can produce large *OmF*s at various time scales (Sinnhuber et al., 2006; Turunen et al., 2009).

Based on the concepts discussed above, we present in Sect. 5 a new diagnostic tool which consists of pressure-time cross sections plots (pressure as vertical coordinate versus time) of means and standard deviations of passive (without chemical assimilation) versus active (with chemical assimilation) *OmF*s for long-lived species such as NO_2, HNO_3, O_3 and CH_4. Daily zonal averages are computed to eliminate the diurnal cycle dependence in order to simplify the analysis. Individual cross sections utilize approximately 12–14 vertical bins (between 0.1 and 100 hPa) centered at the tangent MIPAS observations. For both passive and active cases, meteorological assimilation was performed in the GEM-BACH model using conventional data (aircraft, radiosondes, etc) as well as satellite data from the TOVS/AMSU-A instrument covering the troposphere and stratosphere. Only MIPAS temperatures were assimilated above 70 hPa (i.e. no AMSU-A), as this was found to give the best results for temperature, ozone and HNO_3 (M2007; de Grandpré et al., 2009). It is of paramount importance that the meteorology be assimilated in the same way in both cases mentioned above to ensure the close similarity of temperatures and transport in all experiments. With the help of this new tool, we perform the calculation of polar ozone loss based on "targeted partial column" [2], for two different events: 1) an EPP-IE which took place in a rather continuous fashion during the austral winter of 2003 (May–September 2003) and 2) a

[2]This layer is identified using passive *OmF* biases (see Sect. 5).

ACPD
9, 22459–22504, 2009

major SPE ("Halloween" storm) which occurred towards the end of October 2003 and severely impacted the mesosphere and upper stratosphere in the following weeks.

5 Results

5.1 The relation between NO_2 and CH_4

A scatter plot of NO_x against CH_4 from HALOE observations has been examined in the past to track the signature of EPP-IE. The deviation from a linear relationship in the scatter plot of NO_x against CH_4 (high NO_x and low CH_4) indicates an EPP-IE (Randall et al. 2006; Siskind et al., 2000). In Fig. 1a (case without chemical assimilation) and Fig. 1b (case with assimilation), NO_2 is plotted against CH_4 for both MIPAS observations [3] and the model output near 2 hPa for the second half of August 2003 in the Southern Hemisphere (30° S–90° S). These diagrams illustrate different modes (labeled 1, 2 and 3) which characterize different dynamical and photochemical conditions occurring in the stratopause/upper stratosphere region. The day mode (1) is due to the photo-dissociation of NO_2, which reduces its mixing ratios to very low values irrespectively of CH_4. For the second mode (2), low (high) values of CH_4 near 2 hPa correspond to low (high) values of NO_2 since the source of both constituents is normally located in the troposphere. In this particular case, species are well correlated and this explains the tendency to obey a straight line relationship in the species scatter diagram. For the third mode (3), low values of methane correspond to high values of NO_2, which strongly suggests the presence of a mesospheric source of nitrogen which is transported downward within the polar vortex. Such a phenomenon is seen in the MIPAS dataset shown in Fig. 1 and refers to the EPP-IE signature (Randall et al. 2006, 2007). When chemical assimilation is turned on (Fig. 1b), the third mode (3) is now present in both the observations and the model, which confirms that the phenomenon

[3] MIPAS/ESA observations do not include NO_x (NO_2+NO) but only NO_2 which is nevertheless a good proxy for NO_x during the austral winter.

ACPD
9, 22459–22504, 2009

is well captured by our data assimilation system and our resulting chemical analyses. Therefore, Fig. 1 and other similar scatter diagrams are not only useful in identifying EPP phenomena but turn out to be a tool to test the consistency of the model and the assimilation scheme.

5.2 Analysis of an EPP-IE case in 2003 using *OmF* diagnostics

In this section and those which follow, we examine the spatio-temporal distribution of polar *OmF*s. Results are presented for the period 18 August (Julian day 230) to 5 December 2003 (Julian day 340) for the South Pole region (60° S–90° S). The Northern Hemisphere is not examined here since the EPP-IE influence is smaller in this region due to numerous factors including the inter-hemispheric asymmetry of the solar zenith angle, seasonal differences and different offsets of geomagnetic and geographic poles (Jackman et al., 2008) as well as a typical stronger planetary wave regime. In Fig. 2 (top panels) the passive *OmF* plots (without chemical assimilation) show massive downward transport of NO_2 anomalies from the lower mesosphere to the middle stratosphere region. Note that the end of the polar night is approximately indicated by a thin vertical line in the figures. The rate of descent of the anomalies in the stratosphere is approximately depicted by the slope of the dashed line which represents the location of the *OmF* local maximum throughout the period for NO_2 *OmF* (from Fig. 2a, b). Figure 2a also shows that *OmF* is changing sign near the stratopause (around 0.7–1 hPa) about two weeks after the end of the polar night, suggesting a photochemical dependence on the model bias since here *OmF* varies with the solar zenith angle. More interestingly, important *OmF* anomalies persist persisting at lower altitudes (around and below 10 hPa along the dashed line) until about Julian day 300 (end of October) where the polar vortex starts to break up thus eliminating the trace of EPP-NO_x through mixing processes. Anomalies descending into the stratosphere survive longer due to a stronger confinement of the constituents within the polar vortex and to the fact that NO_x photolysis decreases rapidly below the stratopause, which allows the *OmF* excesses of NO_2 to reach lower levels. The similar descent in the time series of *OmF*

ACPD
9, 22459–22504, 2009

standard deviation (Fig. 2b) is another indication of the strength of the EPP-IE signal in the NO_2 measurements. With chemical assimilation, the mean *OmF* (Fig. 2c) almost vanishes and the standard deviation (Fig. 2d) is reduced, particularly along the dashed line which confirms that our assimilation of MIPAS NO_2 measurements successfully incorporates the missing sources of nitrogen during EPP events. The large reduction for the biases and standard deviations following the assimilation of NO_2 (bottom panels) demonstrates the capability of the assimilation system to capture the slow time scale errors (lifetime of a few weeks to a few months) and/or to correct improper initial conditions. However, *OmF* anomalies (for example caused by artefacts linked to the sponge layer) are still apparent near the model top (Fig. 2c, d), which indicates that the assimilation system cannot eliminate those types of fast time scale systematic errors, as pointed out in Sect. 3. For HNO_3 (Fig. 3), some of the findings noted above apply as seen below. The trace of the EPP effects in the middle stratosphere is clear and approximately (but not perfectly) follows the descent rate found for *OmF* NO_2 anomalies below 1 hPa (depicted by the dashed line). We note that, in the particular case of HNO_3, the *OmF* signal also peaks around 30 hPa and becoming very significant towards the end of the polar night (ending around Julian day 255). The latter is attributed to the misrepresentation of denitrification and sedimentation in the model, which is otherwise well captured by the MIPAS instrument. No other major biases are known for the GEM-BACH model for HNO_3 in the absence of EPP phenomena (see M2007 for more details). For HNO_3, the large bias and standard deviation are eliminated and strongly reduced, respectively, by assimilation (bottom panels of Fig. 3). The success of assimilation for HNO_3 suggests that the *OmF* anomalies were not controlled by fast time scales model errors.

We now examine *OmF* plots for ozone (Fig. 4). Note that the small ozone model deficit (positive *OmF* of ~0.2–0.4 ppmv) which cannot be eliminated after assimilation in the upper stratosphere and stratopause regions (Fig. 4c) is attributed to an inaccurate photochemistry (fast time scales errors, i.e. ~1 day or less). The slanted dashed line corresponding to the case of NO_2 (see on Fig. 2a, b) has also been superimposed

ACPD
9, 22459–22504, 2009

on Fig. 4a and b in order to establish some connections: as HNO_3 and NO_2 *OmF* diminish along this line (as shown in Figs. 2a and 3a), ozone *OmF*s slowly change sign after the end of the polar night and then gradually intensify (in absolute value) until the last week of October (~day 300). This suggests a link between NO_2, HNO_3 anomalies and polar ozone loss (see Sect. 5.4 for more details). By the time the NO_2 *OmF* biases have been reduced to background levels (around Julian day 295, Fig. 2a), significant negative ozone *OmF* biases develop (Fig. 4a). This indicates that the chemical origin of the ozone bias is from EPP-NO_x. During the same period, the HNO_3 *OmF* biases (Fig. 3a) slowly decrease (although not as quickly as for NO_2) which also coincides with the build-up of negative ozone *OmF* biases. The region near 10 hPa around Julian day 285 to 295 corresponds to the maximum depletion of ozone (see also Fig. 10). It is clear that there is a change of regime for the chemical constituent anomalies before and after the end of the polar night, which is seen more strongly for ozone and which is attributed to changes in the lifetime of NO_y and HO_x families from darkness to sunlit conditions. These diagrams suggest that the excesses of NO_y are partly converted into NO which contributes to ozone depletion through catalytic reactions when the sun reappears in the polar vortex (see Reactions (R1) and (R2), Appendix A). Figures 2 and 3 also allow the calculation of the e-folding times of *OmF* NO_2 and HNO_3, throughout the descent, which also turn out to be the lifetimes of the HNO_3 and NO_2 constituents themselves in this particular situation. Regression analyses using the following expressions have been conducted to fit *OmF* data to the following curves:

$$OmF(NO_2)(t)=OmF(NO_2)(t_o)\exp(-c_1(t-t_o)) \quad (15)$$

$$OmF(HNO_3)(t)=OmF(HNO_3)(t_o)\exp(-c_2(t-t_o)) \quad (16)$$

where $OmF\ (NO_2)(t)$ denotes the local maximum passive *OmF* for NO_2 at time t, t_o is the starting time expressed in Julian day (e.g day 230) and c_1, c_2, the rates of decrease of the NO_2 and HNO_3 *OmF* anomalies with time. We obtained c_1=0.0183 (R^2=0.83, p<0.01) and c_2=0.0123 (R^2=0.85, p<0.01). The $1/c_1$ e-folding times are about 55

ACPD
9, 22459–22504, 2009

days for the NO_2 *OmF* and about 80 days for the HNO_3 *OmF*, respectively. Those figures are comparable but nevertheless significantly higher than a similar evaluation made by Rinsland et al. (2005) but at higher altitude and for NO_x during February–March 2004 using ACE observations. In any cases, computed time scales involved here are slow, supporting the connection with a successful chemical assimilation and a significant reduction of *OmF* anomalies as shown in Figs. 2–4 (bottom panels) and predicted in Sect. 3. From Fig. 4a (and also Fig. 10) it is interesting to observe that it is also after about 55 days following t_o (i.e. Julian day 285) that ozone depletion becomes maximum (i.e. *OmF* reaches a minimum) which is consistent with the above results. The presence of an anomalous layer for HNO_3 in the upper stratosphere descending and persisting with time into the middle stratosphere has been explained in terms of hydrated ion cluster chemistry (see Reactions R9 and R10, Appendix A) in the upper stratosphere following EPP events (Kawa, 1995; Stiller et al., 2005; Lopez-Puertas et al., 2005; Orsolini et al., 2005; Jackman et al., 2008). Note that Fig. 3a is consistent with the pressure-time cross section for MIPAS HNO_3 as presented by Stiller et al. (2005)(their Fig. 2) and also present in ODIN HNO_3 measurements (figure not shown).

Figure 5 shows the *OmF* diagnosis plots for methane (CH_4). This constituent is considered as a good dynamical tracer which can be used to diagnose the transport characteristic of the model and its assimilation system. Small values of the passive *OmF* mean and standard deviation (Fig. 5a) along the slanted dashed line indicate that no significant dynamic problem is present in the model bias in the middle stratosphere where we have focused our attention so far and where the ozone loss and EPP-IE signature of NO_y occurs. This means that the biases shown above are mostly of chemical nature and not driven by the dynamics. Note that near the stratopause and in the lower stratosphere important O and F mismatches occurring for methane (Fig. 5a) are mainly attributed to imprecise initial conditions or model top artefacts. In any cases, the CH_4 assimilation of MIPAS observations generally significantly improves the results for the systematic biases in the whole domain (Fig. 5c).

ACPD
9, 22459–22504, 2009

5.3 SPE case during boreal winter 2003

Several solar eruptions occurred in October–November 2003 producing an enormous amount of high energy particles which penetrated in the polar atmosphere. One eruption at the end of October 2003, the so-called "Halloween storm" is considered to be the fourth largest in the past half century or so with computed NO_y production in the middle atmosphere of 5.6 Gigamoles (Jackman et al., 2008). This solar flare has led to an extreme distortion of the Van Allen belts (Baker et al., 2004) and left in its wake several geomagnetic storms from mid-November to mid-December producing several episodes of relativistic electron precipitation and auroras (Turunen et al., 2009). Figure 6 reproduces the proton flux data from GOES-11 (http:/www.spwc.noaa.gov) shortly before and after the SPE which maximum peak took place around Julian day 302–303 (29–30 Octpber). It is therefore anticipated that the "Halloween storm" should leave a strong signature in the upper atmosphere with solar proton flux increases to 4 or 5 orders of magnitude above the background (for protons having energy E>10 MeV). Note that protons with E>30 MeV have sufficient energy to reach the stratosphere and produce NO_x/HO_x directly in this region (Turunen et al., 2009) which can catalytically destroy ozone (see Reactions R1–R4, Appendix A). Figures 7 through 9 provide the *OmF* plots for NO_2, HNO_3 and O_3 respectively with and without assimilation, for periods before and after the storm (the day just before the maximum intensity of the storm was felt in the stratosphere is indicated by a thin vertical line, i.e. 28 October or day 301). We will now focus on the North Pole (60° N–90° N) since the South Pole region had experienced only little trace of the SP event of October/November 2003 (Funke et al., 2005; see also Figs. 2 and 3, Sect. 5.2). Immediately after the onset of the "Halloween storm", passive *OmF* means for NO_2 largely exceeding (by at least 2 orders of magnitude) the background values start appearing in the upper domain (Fig. 7a, b). These excesses subsided from the mesosphere into the upper stratosphere and even reached the middle stratosphere by the end of the period. With chemical assimilation, NO_2 biases (Fig. 7c) diminish significantly showing the beneficial impact of assimilation on

ACPD
9, 22459–22504, 2009

the short term forecast. The standard deviations are also slightly reduced for NO_2 with assimilation (Fig. 7d) especially along the slanted dashed line. This line represents the rate of descent of the NO_2 *OmF* anomalies within the polar vortex which can now be used as a proxy for atmospheric subsidence in the region. It is thus evaluated at about 11 km per month which results in a significant downward transport of the chemical perturbation following the event. This value is higher but in the same range as found by other authors (Rinsland, 2005; Manney, 1994) under similar conditions. Using the same methodology as in the previous section, a least square fit to the following expression:

$OmF(NO_2)(t)=OmF(NO_2)(t_o)\exp(-c_3(t-t_o))$ gives $c_3=0.0315$ with $R^2=0.82$ ($p<0.01$). The e-folding time $1/c_3\sim30$ days is about two times smaller here than for the EPP-IE case (Sect. 5.2) but is now in agreement with the results of Risland et al. (2005) obtained for NO_x. The shorter time scale obtained for NO_2 as compared to the EPP-IE case is due to the location of the maximum *OmF* biases now at a higher altitude where the lifetime of NO_2 is smaller (Brasseur and Solomon, 2005). *OmF* for HNO_3 (Fig. 8a, b) show significant excesses in the 1–2 hPa layer (labeled as 1) and appearing right after the onset of SPE. Note that there were no MIPAS-ESA data available above 1 hPa to be assimilated for HNO_3. It is very likely that this excess in HNO_3 *OmF* in the stratopause/upper stratosphere region is the signature of fast gas phase chemistry (Reactions R6–R8, Appendix A) and/or ion recombination chemistry (Reaction R5 in Appendix A) following the production of NO_x and HO_x during EPP (Brasseur and Solomon, 2005; Lopez-Puertas et al., 2005; Jackman et al., 2008). Although the gas phase Reactions R6–R8 are included in our model, the lack of assimilation of HO_x and NO produces the HNO_3 *OmF* trace which appears near 1 hPa on Fig. 8a and b. A secondary maximum of mean HNO_3 *OmF* in November (labeled as 2) appears at about 2 hPa near Julian day 325 to 340 and is associated with the production and downward transport of NO_x which reaches the 1 hPa level about 1 month after the onset of the SPE event. The rate of descent (indicated by the dashed line) has been superimposed from *OmF* NO_2 plots. During the descent,

ACPD
9, 22459–22504, 2009

active nitrogen compounds are converted into HNO_3. One process likely involved is the ion cluster chemistry which takes place over a time scale of about 1 month in this strongly ionized atmosphere (Lopez-Puertas, 2005; Stiller et al., 2005; Kawa et al., 1995; Orsolini et al., 2005). The latter is consistent with the large maximum mean HNO_3 *OmF* in that region. The e-folding time computed above (~30 days) matches this time scale of processes associated with the theory of ion cluster chemistry for NO_2 decrease. In the middle and low stratosphere, important model errors also exist (labeled 3 and 4 on Fig. 8a, b) with sharp and persistent mean *OmF* maximum for HNO_3 particularly around 20–30 hPa during the period. The latter phenomenon is not related to any SPE event and could be explained by some model deficiencies regarding NO_y partitioning in the region. But the origin of the secondary maximum labeled 3 is not clear and could be associated with slow time processes such as ion cluster chemistry since assimilation reduces significantly its trace (Fig. 8c, d). This type of heterogeneous chemistry is usually effective at higher altitude but during this SPE Jackman et al. (2008)(their Fig. 1) showed that large ionization rates were produced down to 10 hPa.

Therefore, Figs. 7 and 8 indicate that the nature of the errors is mostly associated with initial conditions or slow time scale modeling errors. Note that signature of SPE persisting after assimilation (bottom panels) in the upper stratosphere and stratopause regions (labeled as 1 or 2 in top panels) would indicate, in principle, fast time scale model errors. However, for the region labeled as 2, it is not possible to confirm this evaluation since there were no data to assimilate above 1 hPa where the air originated from. On the contrary, Jackman et al. (2008) demonstrated that a buildup of N_2O_5 (a precursor of HNO_3, see Reactions R9–R10, Appendix A) takes place in that region associated with the same event which then supports the presence of ion cluster chemistry as discussed above.

Coincident with excesses for the NO_y family in the region 1–2 hPa, a reduction of the ozone *OmF* mean (Fig. 9a) is clearly noted after the onset of SPE with the lowest value occurring around days 320–330. *OmF* biases are about 0.2 to 0.6 ppmv shortly before

day 301 and fall to near zero following the SPE (see also figure 11). This reduction demonstrates its sensitivity to the NO_y background conditions in the region. The positive ozone model bias which appears in the background in the upper stratopause/upper stratosphere region (0.5–2 hPa) throughout the whole period (from day 230 to 340) is linked to a known misrepresentation of the photochemistry (M2007) as in the case of EPP-IE in the Southern Hemisphere. Finally, at the model top, assimilation has little effect due to fast time scale errors linked with the sponge as previously noted.

5.4 Calculation of the polar ozone loss due to EPP based on *OmF*s

In this section, we evaluate the stratospheric ozone loss partial column for the cases studied previously in Sects. 5.2 and 5.3 with the help of the *OmF* cross sections. Figure 10 shows time series of the passive *OmF* biases for O_3, NO_2 and HNO_3 at the 14.5 hPa level for the EPP-IE case described in Sect. 5.2. This level was selected since it corresponds to the maximum impact of EPP (maximum absolute value of mean *OmF* biases) of ozone. During the polar night (Julian day 230–255) *OmF* biases for NO_2 and HNO_3 and ozone display a weak positive correlation whereas when the polar region is illuminated but the polar vortex still present in the lower stratosphere (day 270–315), the relationship is changed to a negative correlation (see Table 1 for details). The increase of *OmF* biases for NO_2 starting around Julian day 270 is clearly related to the increase brought by the vertical transport in the polar vortex (as shown by the dashed line in Fig. 2 through 4) combined with the presence of sunlight. The drop (increase) of the ozone *OmF* biases is anti-correlated to the rise (drop) of *OmF* biases for NO_2 and to a certain extent to *OmF* biases for HNO_3 after Julian day 255 (when illumination approximately starts at the polar cap). The resulting time variation of the "targeted ozone partial column" (in DU units) of *OmF* biases between 7 and 30 hPa is also computed and provided in Fig. 10 (magenta curve). The difference between Julian days 230–255 (during the polar night) and the period after (days 285–315 just before the vortex breakup) was found to be 5.5±2.8 DU (Dobson unit). This is believed to be the average impact (over about 1 month period) of the EPP-IE event on the reduction of the

ACPD
9, 22459–22504, 2009

ozone column over the South Pole region. Table 1 summarizes the results. This estimate could be compared with an evaluation of WMO (2007) on ozone depletion where the impact due to EPP was determined to be less than 10 DU. We now apply the same methodology but for the SPE case. Figure 11 depicts time series of O_3, NO_2 and HNO_3 and partial ozone column for *OmF* biases at an appropriate level (i.e. 1.585 hPa in this case) based on plots of Fig. 9 for the North Pole region. The biggest increase of *OmF* biases for NO_2 occurs just after the SPE (Julian day 301) as expected (consistent with Figs. 6 and 7a). The "target partial column" where the depletion takes place is now from 0.5 to 4 hPa (based on Fig. 9a). The difference between the ozone partial column *OmF* biases before and after the SPE is evaluated, as an average, to 0.8±0.5 DU (which is much smaller than that for the EPP-IE case). The lesser confinement in the NH polar vortex and the high altitude (near 1 hPa) of the ozone loss where the air density is weak explains the small impact on the ozone column. We have conducted sensitivity tests on the depth of the "target layer" used to make calculations of polar ozone loss in both cases (EPP-IE and SPE) without much difference in the results. A significant anti-correlation between *OmF* biases for NO_2 and O_3 ($R=-0.59$) develops after the onset of SPE illustrating the role of NO_x in ozone destruction. Table 2 summarizes the correlations between species for the SPE event. Ozone is also affected by HO_x production from EPP (Reactions R3–R4, Appendix A) but the study of this family of constituents is beyond the scope of this paper since no measurement is available. Moreover, its effect is transient and has a smaller impact after the end of the polar night due to their fast photochemical time scales.

An alternative method for computing the polar ozone loss would be to subtract the total column of the passive from the active case. The latter approach has been apparently successful in evaluating the polar loss due to heterogeneous chemistry in the polar vortex (Orsolini, 2008). However, in the context of our study, total column differences were found unrealistic. This could be explained by the following reasons: 1) the signal/noise ratio of EPP impacts is likely to be low in the lower stratosphere, 2) the total column variations between the two cases could be due to other factors (e.g. chemistry

ACPD
9, 22459–22504, 2009

biases, observation and retrievals errors, etc.) not linked to EPP, and 3) total column calculations are particularly sensitive to errors in the lower stratosphere where air density is higher. The polar loss from EPP can also be estimated without any reference to chemical monitoring or assimilation as done by other authors. However, it requires costly and complex modeling or parameterization of coupled ion-neutral chemistry, ion drag and auroral processes, non-LTE effects, shortwave heating at extreme ultraviolet wavelength (see Brasseur and Solomon, 2005; Jackman et al., 2008), a higher model top (at least in the MLT region), EPP sources modeling (Jackman et al., 2008; Semeniuk et al., 2005) and ion cluster chemistry (Brasseur and Solomon, 2005; Kawa, 1995) or involving long model integrations (Rozanov et al., 2005) or necessitated extensive multiyear comparison of observations under different meteorological conditions (Randall et al., 2006, 2007). Use of both passive and active *OmF*s as an alternative method demands less complexity while providing significant insight on the impact of EPP events.

6 Summary and conclusions

The GEM-BACH coupled dynamical-chemical data assimilation system has been used to ingest MIPAS NO_2, O_3, HNO_3, CH_4 and temperature during two EPP (energetic particle precipitation) events that occurred in 2003 (EPP-IE during austral winter and SPE during boreal winter). To the best of our knowledge, it is the first time that chemical data assimilation has been successful in capturing the EPP signal within the polar vortices or elsewhere. Errera et al. (2008) have assimilated MIPAS-ESA for a longer period covering different EPP events but did not succeed in capturing NO_y produced by EPP. In our study, an estimation of the error variances (based on the H-L method adapted to satellite data) and a relaxed quality control prevented the rejection of large (but valid) NO_2 and HNO_3 *OmF* residuals associated with EPP events. This demonstrates the high importance of prescribing error statistics prior to assimilation in a rigorous way and using an appropriate relaxed quality control, as was done in this study.

ACPD
9, 22459–22504, 2009

The chemical signature of EPP events has been analyzed and diagnosed with a new tool using both passive (without assimilation) and active (with assimilation) *OmF* cross sections. The passive *OmF*s filter out processes that the model simulates well and thus better isolate anomalies such as excesses in NO_y due to EPP impacts within the polar vortices which are not provided by the model. Combined passive and active *OmF*s offer a tool which permits an assessment of the nature of the *OmF* residuals and their e-folding time (i.e. errors due to the initial conditions and modeling errors at various time scales). The tool also turns out to be a useful method for model and assimilation assessment. Our results indicate delays of about one month or so, identified on different occasions between the maximum *OmF* biases for NO_2 and the build-up of *OmF* biases for HNO_3, suggesting the possibility of the occurrence of slow time scale reactions, such as those involved in heterogeneous ion cluster chemistry. These chemical processes are absent from current stratospheric chemistry models. Finally, using a method based on the "target partial column", we were able to infer the impact of EPP on the stratospheric polar ozone loss by using time series of the passive *OmF* biases. The average impact on total column ozone depletion for the South Pole (latitude $> 60^{o}$S) has been estimated to be about 5–6 DU for the EPP-IE case during Antarctic winter 2003. This represents up to 5% of the value of the total column ozone found in the ozone hole. For the SPE case, the chemically induced ozone loss was modest compared to the EPP-IE and was determined to be about 1 DU. Therefore, despite stronger geomagnetic effects associated to SPE, the resulting ozone depletion is less important in the NH case as compared to the SH EPP-IE case during austral winter. The reason for this is linked to: 1) a weaker and less confined polar vortex in the NH than the SH, and 2) a possible lack of favorable synchronism of meteorological conditions after the onset of the SPE favoring strong descent (see Randall et al., 2006, 2007; Seppälä, 2007; Siskind et al., 2007; Turunen et al., 2009). Consequently, for the SPE case, ozone depletion mostly took place in the higher stratosphere and mesosphere, which had little impact on the total ozone column. Finally, one consequence of our work is that, from an assimilation point of view, slow time scale modeling errors or

ACPD
9, 22459–22504, 2009

initial condition errors play a secondary role in the stratosphere and that a correction of the chemical concentrations via careful assimilation is adequate to provide a realistic chemical analysis. We leave for future work the application of the methods shown in this paper for other EPP cases and also to other phenomena not included in models but captured by assimilation.

Appendix A

List of important chemical reactions (discussed in the text)

NO_x catalytic reactions

$$NO + O_3 \rightarrow NO_2 + O_2 \quad \text{(R1)}$$

$$NO_2 + O \rightarrow NO + O_2 \quad \text{(R2)}$$

HO_x catalytic reactions

$$OH + O_3 \rightarrow HO_2 + O_2 \quad \text{(R3)}$$

$$HO_2 + O \rightarrow OH + O_2 \quad \text{(R4)}$$

ACPD
9, 22459–22504, 2009

Ion recombination chemistry

$$H_2O + NO_3 \rightarrow HNO_3 + OH \quad \text{(R5)}$$

(requires ion and darkness)

Gas phase chemistry

$$NO_2 + OH + M \rightarrow HNO_3 + M \quad \text{(R6)}$$

$$HNO_3 + OH \rightarrow NO_3 + H_2O \quad \text{(R7)}$$

$$HNO_3 + h\nu \rightarrow NO_3 + H_2O \quad \text{(R8)}$$

Ion cluster chemistry (time scale of about 1 month)

$$NO_2 + NO_3 + M \rightarrow N_2O_5 + M \quad \text{(R9)}$$

(thermal decomposition reaction)

$$N_2O_5 + H_2O(\text{ion cluster}) \rightarrow 2HNO_3 \quad \text{(R10)}$$

Acknowledgements. The authors wish to thank ESA contract officer Tobias Weir for his direction and encouragements during our early work on this paper (through an European Space Agency contract), Paul-André Beaulieu for providing the MIPAS observations in the appropriate format and to Alexander Kallaur and Vivian Lee for their work on the chemistry interface of the GEM-BACH model.

References

Baier, F., Erbertseder, T., Morgenstern, O., Bittner, M., and Brasseur, G.: Assimilation of MIPAS observations using a three-dimensional global chemistry-transport model, Q. J. Roy. Meteorol. Soc., 613, 3529–3542, 2005.

Baker, D. N., Kanekal, S. G., Li, X., Monk, S. P., Goldstein, J., and Burch, J. L.: An extreme distortion of the Van Allen belt arising from the "Halloween" solar storm in 2003, Nature, 432, 878–880, 2004.

Brasseur, G. and Solomon, S.: Aeronomy of the Middle Atmosphere: Chemistry and Physics of the Stratosphere and Physics of the Stratosphere and Mesosphere, Third revised and enlarged ed., Springer, ISBN 978-1-4020-3284-4, 2005.

Callis, L. B., Baker, D. N., Natarajan, M., Blake, J. B., Mewaldt, R. A., Selesnick, R., and Cummings, J. R.: A 2-D model simulation of downward transport of NO_y into the stratosphere: Effects on the 1994 austral spring O_3 and NO_y, Geophys. Res. Lett., 23, 1905–1908, 1996.

Côté, J., Gravel, S., Méthot, A., Patoine, A., Roch, M., and Staniforth, A. N.: The operational CMC-MRB Global Environmental Multiscale (GEM) model, Part I: design considerations and formulation, Mon. Weather Rev., 126, 1373–1395, 1998.

Daley, R.: Atmospheric data analysis, Cambridge University Press, 1991.

Damian, V., Sandu, A., Damian, M., Potra, F., and Carmichael, G. R.: The kinetic preprocessor KPP – a software environment for solving chemical kinetics, Comput. Chem. Eng., 26, 1567–1579, 2002.

Dee, D. P. and da Silva, A. M.: Data assimilation in the presence of forecast bias, Q. J. Roy. Meteorol. Soc., 124, 269–295, 1998.

de Grandpré, J., Ménard, R., Rochon, Y. J., Charrette, C., Chabrillat, S., and Robichaud, A.: Predictability of coupled chemistry-dynamics data assimilation, Mon. Weather Rev., 137, 679–692, 2009.

Dethof, A.: Assimilation of ozone retrievals from the MIPAS instrument on board ENVISAT, ECMWF Technical Memorandum, 428, 2003.

Dethof, A., Geer, A., Lahoz, W., Goutail, F., Bazureau, A., Wang, D. Y., and von Clarmann, T.: MIPAS temperature validation by the MASI group, ESA, in: Proceedings of the Second Workshop on the Atmospheric Chemistry Validation of ENVISAT (ACVE-2), ESA-ESRIN, Frascati, Italy (ESA SP-562), 3–7 May 2004, 23.1–23.5, 2004.

Errera, Q. and Fonteyn, D.: Four-dimensional variational chemical assimilation of CRISTA

stratospheric measurements, J. Geophys. Res., 106, 12253–12265, 2001.
Errera, Q., Daerden, F., Chabrillat, S., Lambert, J. C., Lahoz, W. A., Viscardy, S., Bonjean, S., and Fonteyn, D.: 4D-Var assimilation of MIPAS chemical observations: ozone and nitrogen dioxide analyses, Atmos. Chem. Phys., 8, 6169–6187, 2008, http://www.atmos-chem-phys.net/8/6169/2008/.
ESA (European Space Agency): ENVISAT, MIPAS, An instrument for atmospheric chemistry and climate research, ESA Publications Division, ESTEC, P.O. Box 299, 2200 AG Noordwijk, The Netherlands, SP-1229, 2000.
Fischer, H. and Oelhaf, H.: Remote sensing of vertical profiles of atmospheric trace constituents with MIPAS limb-emission spectrometers, Appl. Optics, 35, 2787–2796, 1996.
Fischer, H., Birk, M., Blom, C., Carli, B., Carlotti, M., von Clarmann, T., Delbouille, L., Dudhia, A., Ehhalt, D., Endemann, M., Flaud, J. M., Gessner, R., Kleinert, A., Koopman, R., Langen, J., López-Puertas, M., Mosner, P., Nett, H., Oelhaf, H., Perron, G., Remedios, J., Ridolfi, M., Stiller, G., and Zander, R.: MIPAS: an instrument for atmospheric and climate research, Atmos. Chem. Phys., 8, 2151–2188, 2008, http://www.atmos-chem-phys.net/8/2151/2008/.
Funke, B., López-Puertas, M., Gil-López, S., von Clarmann, T., Stiller, G. P., Fischer, H., and Kellmann, S.: Downward transport of upper atmospheric NO_x into the polar stratosphere and lower mesosphere during the Antarctic 2003 and Arctic 2002/2003 winters, J. Geophys. Res., 110, D24308, doi:10.10129/2005JD006463, 2005.
Gauthier, P., Charrette, C., Fillion, L., Koclas, P., and Laroche, S.: Implementation of a 3D variational data assimilation system at the Canadian Meteorological Centre, Part I: The global analysis, Atmos. Ocean, 37, 103–156, 1999.
Gauthier, P., Chouinard, C., and Brasnett, B.: Quality control: Methodology and applications, in: Data Assimilation for the Earth System, edited by: Swinbank, R., Shutyaev, V., and Lahoz, W. A., NATO Science Series IV: Earth and Environment Science, Kluwer Academic Publishers, 26, 177–187, 2003.
Hairer, E. and Wanner, G.: Solving ordinary differential equations 2 – Stiff and differential-algebraic problems, Springer series in computational mathematics, Springer, Second edition, 14, 1996.
Hollingsworth, A. and Lönnberg P.: The statistical structure of short-range forecast errors as determined from radiosonde data, Part I, The wind field, Tellus, 38A, 111–136, 1986.
Jackman, C. H., McPeters, R. D., Labow, G. J., Fleming, E. L., Praderas, C. J., and Russell,

J. M.: Northern hemisphere atmospheric effects due to the July 2000 Solar Proton Event, Geophys. Res. Lett., 28(15), 2883–2886, 2001.
Jackman, C. H. and McPeters, R. D.: The Effect of Solar Proton Events on Ozone and Other Constituents, in: Solar Variability and its Effects on Climate, edited by: Pap, J. M., Fox, P., Frohlich, C., Hudson, H. S., Kuhn, J., McCormack, J., North, G., Sprigg, W., and Wu, S. T., AGU, Washington DC, Geophy. Monog. Series, 141, 305–319, 2004.
Jackman, C. H., Marsh, D. R., Vitt, F. M., Garcia, R. R., Fleming, E. L., Labow, G. J., Randall, C. E., López-Puertas, M., Funke, B., von Clarmann, T., and Stiller, G. P.: Short- and medium-term atmospheric constituent effects of very large solar proton events, Atmos. Chem. Phys., 8, 765–785, 2008, http://www.atmos-chem-phys.net/8/765/2008/.
Kalnay, E.: Atmospheric Modeling, Data Assimilation and Predictability, Cambridge University Press, 2003.
Kawa, S. R., Kumer, J. B., Douglass, A. R., Roche, A. E., Smith, S. E., Taylor, F. W., and Allen, D. J.: Missing chemistry of reactive nitrogen in the upper stratospheric polar winter, Geophys. Res. Lett., 22, 2629–2632, 1995.
López-Puertas, M., Funke, B., Gil-López, S., von Clarmann, T., Stiller, G. P., Höpfner, M., Kellmann, S., Fischer, H., and Jackman, C. H.: Observation of NO_x enhancement and ozone depletion in the Northern and Southern Hemispheres after the October–November 2003 solar proton events, J. Geophys. Res., 110, A09S43, doi:10.1029/2005JA011050, 2005.
Manney, G. L., Zurek, R. W., O'Neill, A., and Swinbank, R.: On the motion of air through the stratospheric polar vortex, J. Atmos. Sci., 51, 2973–2994, 1994.
Ménard, R., Gauthier, P., de Grandpré, J., Robichaud, A., Rochon, Y., Chabrillat, S., Fonteyn, D., von Clarmann, T., Yang, Y., Charron, M., McConnell, J., Kaminski, J., Vaillancourt, P., Charrette, C., Kallaur, A.: Coupled chemical-dynamical data assimilation, executive summary available at http://esamultimedia.esa.int/docs/gsp/completed/C18560ExS.pdf, ESA/ESTEC Contract No. 18560/04/NL/FF, 2007.
Ménard, R.: Bias estimation, in: Data assimilation, edited by: Lahoz, W., Khattatov, B., and Ménard, R., Springer, 2009.
Orsolini, Y. J., Manney, G. L., Santee, M., Randall, C. E.: An upper stratospheric layer of enhanced HNO_3 following exceptional solar storms, Geophys. Res. Lett., 32(12), L12S01, doi:10.129/2004GL021588, 2005.
Orsolini, Y. J.: Arctic ozone loss inferred from assimilation of MLS and SBUV observations, 37th

COSPAR Scientific Assembly, Montreal, Canada, 13–20 July 2008, A11-0078-08, 2008.
Parrish, D. F. and Derber, J. C.: The National Meteorological Center's Spectral Statistical-Interpolation Analysis System, Mon. Weather Rev., 120, 1747–1763, 1992.
Polavarapu, S., Ren, S., Rochon, Y., Sankey, D., Ek, N., Koshyk, J., and Tarasick, D.: Data assimilation with the Canadian Middle Atmosphere Model, Atmos. Ocean, 43(1), 77–100, 2005.
Randall, C. E., Harvey, V. L., Singleton, C. S., Bernath, P. F., Boone, C. D., and Kozyra, J. U.: Enhanced NO_x in 2006 linked to strong upper stratospheric Arctic vortex, Geophys. Res. Lett., 33, L18811, doi:10.1029/2006GL027160, 2006.
Randall, C. E., Harvey, V. L., Singleton, C. S., Bailey, S. M., Bernath, P. F., Codrescu, M., Nakajima, H., and Russell, J. M.: Energetic particle precipitation effects on the Southern Hemisphere stratosphere in 1992–2005, J. Geophys. Res., 112, D08308, doi:10.1029/2006JD007696, 2007.
Rinsland, C. P., Boone, C., Nassar, R., Walker, K., Bernath, P., McConnell, J. C., and Chiou, L.: Atmospheric Chemistry Experiment (ACE), Arctic stratospheric measurements of NO_x during February and March 2004: Impact of intense solar flares, Geophys. Res. Lett., 32, L16S05, doi:10.1029/2005GL022425, 2005.
Rozanov, E., Callis, L., Schlesinger, M., Yang, F., Andronova, N., and Zubov, V.: Atmospheric response to NO_y source due to energetic electron precipitation, Geophys. Res. Lett., 32, L14811, doi:1029/2005GL023041, 2005.
Sander, S. P., Friedl, R. R., Golden, D. M., Kurylo, M. J., Huie, R. E., Orkin, V. L., Moortgaat, G. K., Ravishankara, A. R., Kolb, C. E., Molina, M. J., and Finlayson-Pitts, B. J.: Chemical Kinetics and Photochemical Data for Use in Atmospheric Studies, Evaluation Number 14, Publication 02–25, JPL, 2003.
Semeniuk, K., McConnell, J. C., and Jackman, C. H.: Simulation of the October–November 2003 solar proton events in the CMAM GCM: Comparison with observations, Geophys. Res. Lett., 32, L15S02, doi:10.1029/2005GL022392, 2005.
Seppälä, A., Verronen, P. T., Kyrölä, E., Hassinen, S., Backman, L., Hauchecorne, A., Bertaux, J. L., and Fussen, D.: Solar proton events of October–November 2003: Ozone depletion in the Northern Hemisphere polar winter as seen by GOMOS/Envisat, Geophys. Res. Lett., 31(19), L19107, doi:10.1029/2004GL021042, 2004.
Seppälä, A., Verronen, P. T., Cliverd, M. A., et al.: Arctic and Antarctic polar vortex NO_x and energetic particle precipitation in 2002–2006, Geophys. Res. Lett., 34, L12810,

doi:10.1029/2007GL029733, 2007.
Sinnhuber, B.-M., von der Gathen, P., Sinnhuber, M., Rex, M., König-Langlo, G., and Oltmans, S. J.: Large decadal scale changes of polar ozone suggest solar influence, Atmos. Chem. Phys., 6, 1835–1841, 2006, http://www.atmos-chem-phys.net/6/1835/2006/.
Siskind, D. E., Nedoluha, G. E., Randall, C. E., Fromm, M., and Russell, III, J. M.: An assessment of Southern Hemisphere stratospheric NO_x enhancements due to transport from the upper atmosphere, Geophys. Res. Lett., 27, 329–332, 2000.
Siskind, D. E., Eckermann, S. D., Coy, L., McCormack, J. P., and Randall, C. E.: On recent interannual variability of the Arctic winter mesosphere: Implications for tracer descent, Geophys. Res. Lett., 34, L09806, doi:10.1029/2007GL029293, 2007.
Solomon, S. and Crutzen, P. J.: Analysis of the August 1972 solar proton event including chlorine chemistry, J. Geophys. Res., 86, 1140–1151, 1981.
Stiller, G. P., Gizaw, M. T., von Clarmann, T., Glatthor, N., Höpfner, M., Kellmann, S., Linden, A., Ruhnke, R., Fischer, H., López-Puertas, M., Funke, B., and Gil-López, S.: An enhanced HNO_3 second maximum in the Antarctic midwinter upper stratosphere 2003, J. Geophys. Res., 110, D20303, doi:10.1029/2005JD006011, 2005.
Turunen, E., Verronen, P. T., Seppälä, A., Rodger, C. J., Clilverd, M. A., Tamminen, J., Enell, C. F., and Ulich, T.: Impact of different energies of precipitating particles on NO_x generation in the middle and upper atmosphere during geomagnetic storms, J. Atmos. Sol.-Terr. Phy., 71, doi:10,1016/j.jastp.2008.07.05, 2009.
von Clarmann, T.: Personal discussion at ESTEC (Netherlands), 2007.
Wang, D. Y., von Clarmann, T., Fischer, H., et al.: Validation of stratospheric temperatures measured by Michelson Interferometer for Passive Atmospheric Sounding (MIPAS) on Envisat, J. Geophys. Res., 110, D08301, doi:10.1029/2004JD005342, 2005.
WMO: Scientific Assessment of Ozone Depletion: 2006, Global Ozone Research and Monitoring, Project-Report No. 50, World Meteorological Organization, Geneva, 2007.

Table 1. Average *OmF* correlation coefficients and average ozone *OmF* partial columns for the EPP-IE case during the polar night (before day 255) and under illumination (day 285–315).

	Before day 255	Day 285–315	Difference
Avg. partial column of *OmF* biases (DU):	3.03±0.90	−2.43±1.92	5.5±2.8
Correlation coefficient: for NO_2 vs O_3	0.18**	−0.66	Change of sign
OmF biases HNO_3 vs O_3	0.34**	−0.63	Idem
NO_2 vs HNO_3	−0.52*	0.96	Idem

* Correlation coefficient statistically significant with a level of confidence above 95%.
** Not statistically significant above 95%.
Otherwise, statistically significant above 99%.

ACPD
9, 22459–22504, 2009

Table 2. Average *OmF* correlation coefficients and average ozone *OmF* partial columns for the SPE case shortly before and after the onset of the SPE.

	Shortly before day 301	Day 305–332	Difference
Avg. partial column *OmF* biases (DU)	0.86±0.14	−0.05±0.34	0.91±0.48
Correlation coefficient for NO_2 vs O_3	N/S	−0.59	N/A
OmF biases			
HNO_3 vs O_3	N/S	−0.11**	N/A
NO_2 vs HNO_3	−0.63**	0.27**	Change of sign

N/S: No correlation (not significant), N/A: non applicable.
** Not statistically significant above 95%.
Otherwise, statistically significant above 99%.

ACPD
9, 22459–22504, 2009

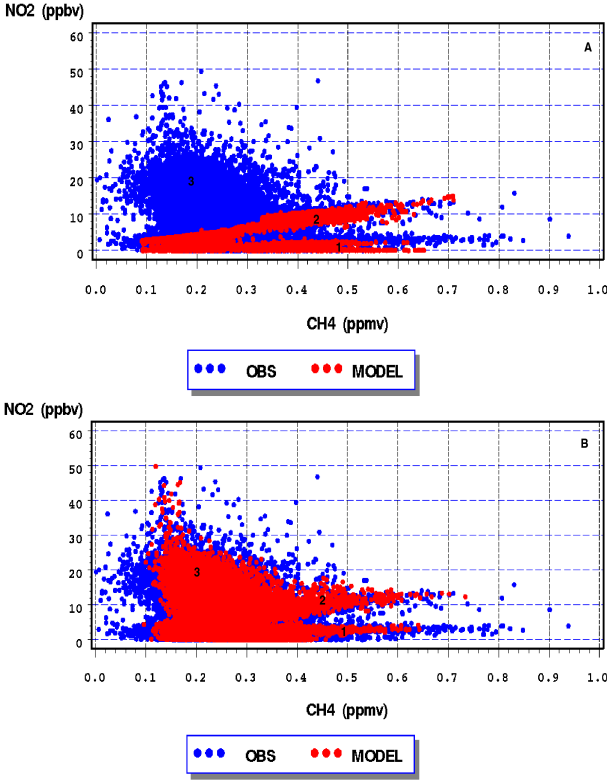

Fig. 1. Scatter diagram of NO_2 versus CH_4 for the Southern Hemisphere (30° S–90° S) around 2 hPa for MIPAS observations (blue) and model outputs (red): **(A)** without chemical assimilation, **(B)** with chemical assimilation, 1: day mode, 2: nocturnal mode, 3: EPP signature.

ACPD
9, 22459–22504, 2009

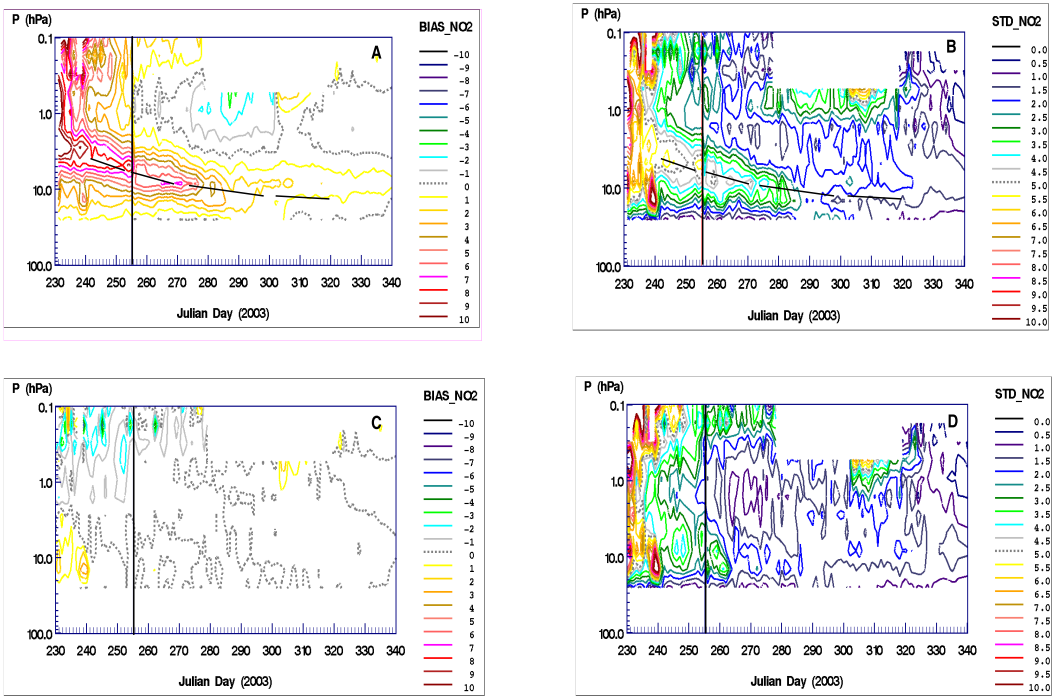

Fig. 2. Pressure-time plots of NO_2 *OmF* in ppbv. Top panels: no chemical assimilation, **(A)** biases, **(B)** std. dev. Bottom panels: **(C)** and **(D)** are identical to (A) and (B) respectively but with chemical assimilation included. The domain is the South Pole region (latitudes >60° S). The vertical line roughly indicates the end of the polar night and the slanted black dashed line, the rate of descent for the local maximum of *OmF*. A period of missing data is present above 5 hPa during the period from day 280 to 320 for all constituents. Note also that no data is available for NO_2 below about 25 hPa.

ACPD
9, 22459–22504, 2009

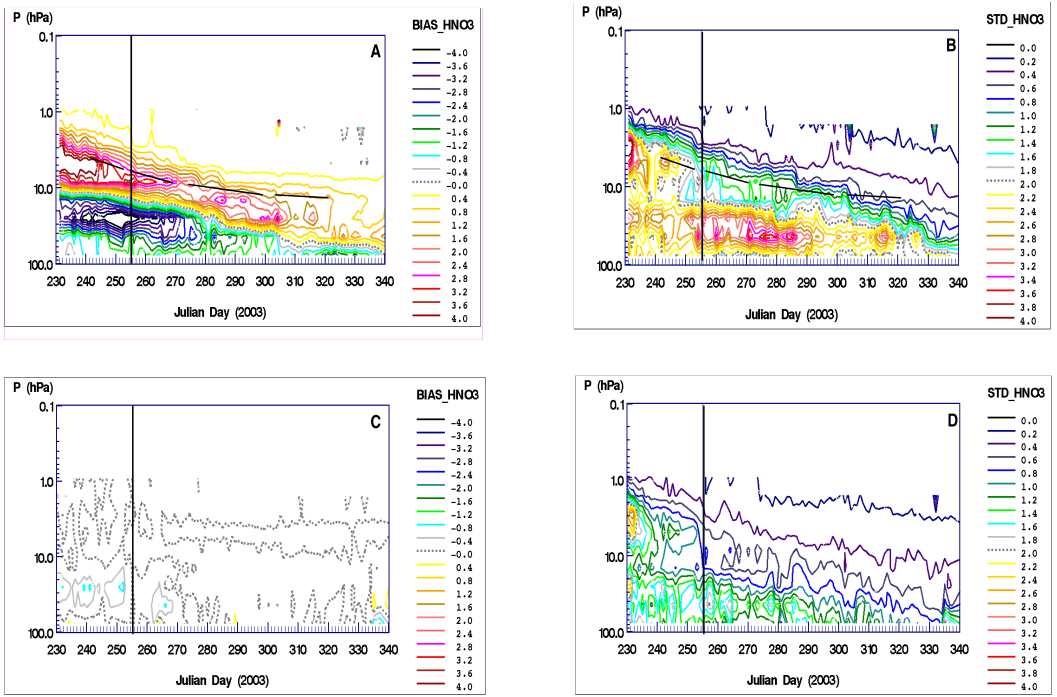

Fig. 3. As Fig. 2 but for HNO_3: Top (without assimilation), bottom (with assimilation), left (bias), right (std. dev.). The rate of descent of NO_2 *OmF* (dashed line) is superimposed for comparison. No data is available for HNO_3 above roughly 1 hPa.

ACPD
9, 22459–22504, 2009

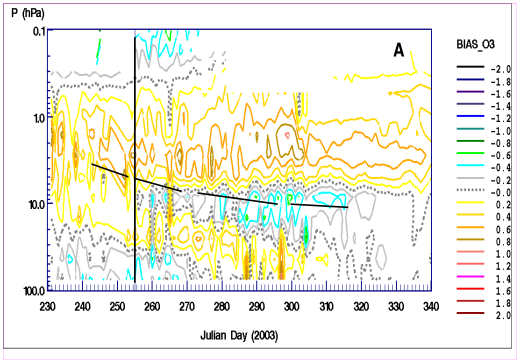

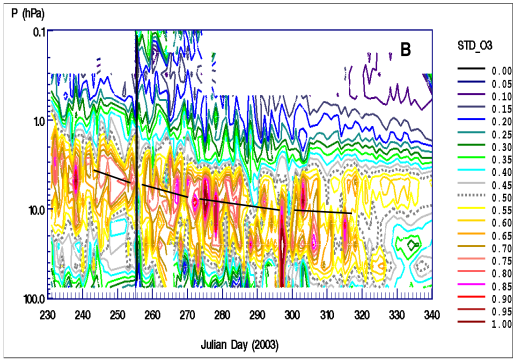

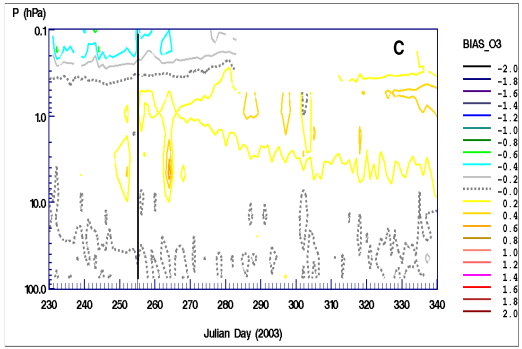

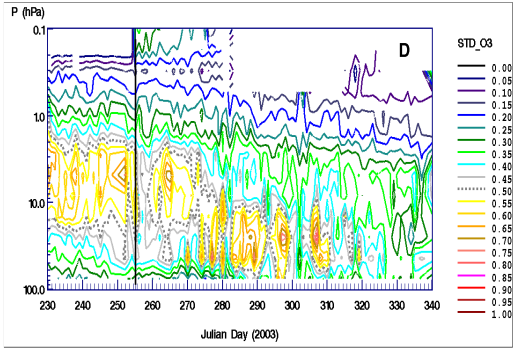

Fig. 4. As Fig. 2 but for O_3 (units are ppmv).

ACPD
9, 22459–22504, 2009

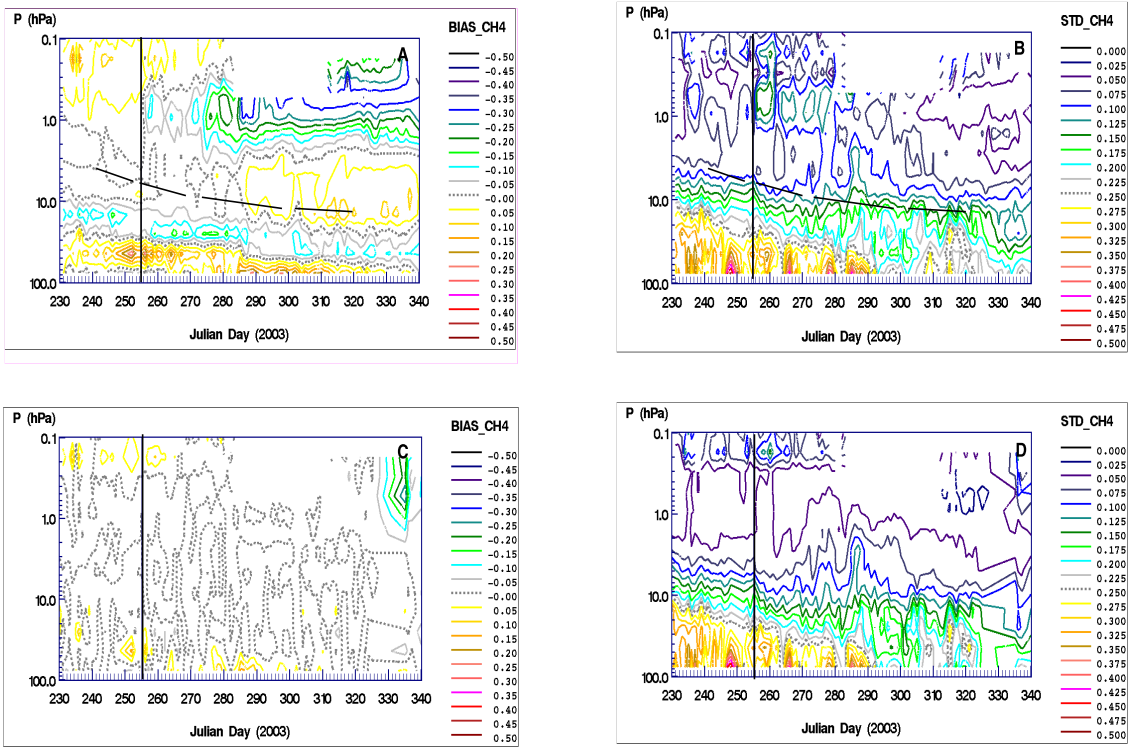

Fig. 5. As Fig. 4 but for CH_4 (units are ppmv).

ACPD
9, 22459–22504, 2009

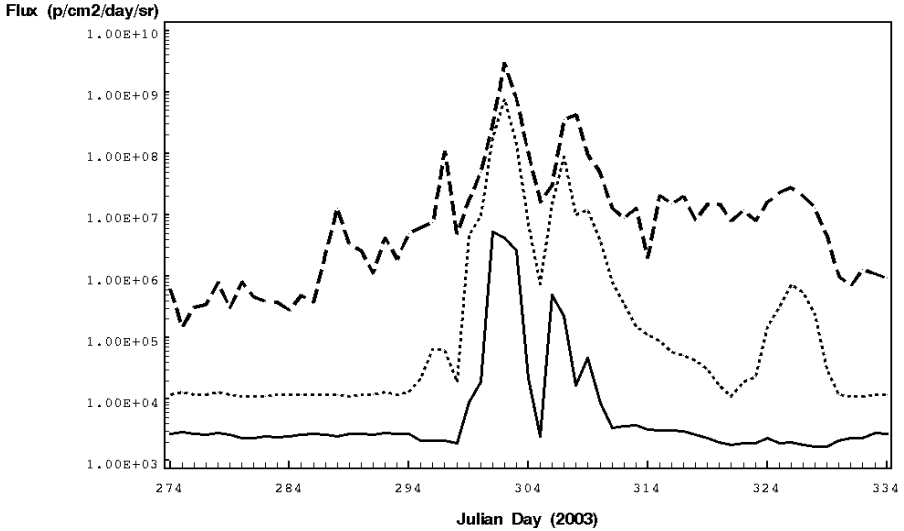

Fig. 6. Solar proton flux measurements by GOES-11 (October–November 2003) for protons having energy >1 MeV (black dashed), 10 MeV (thin dashed) and 100 MeV (solid black). The unit for fluxes is protons/cm^2/day/steradian.

ACPD
9, 22459–22504, 2009

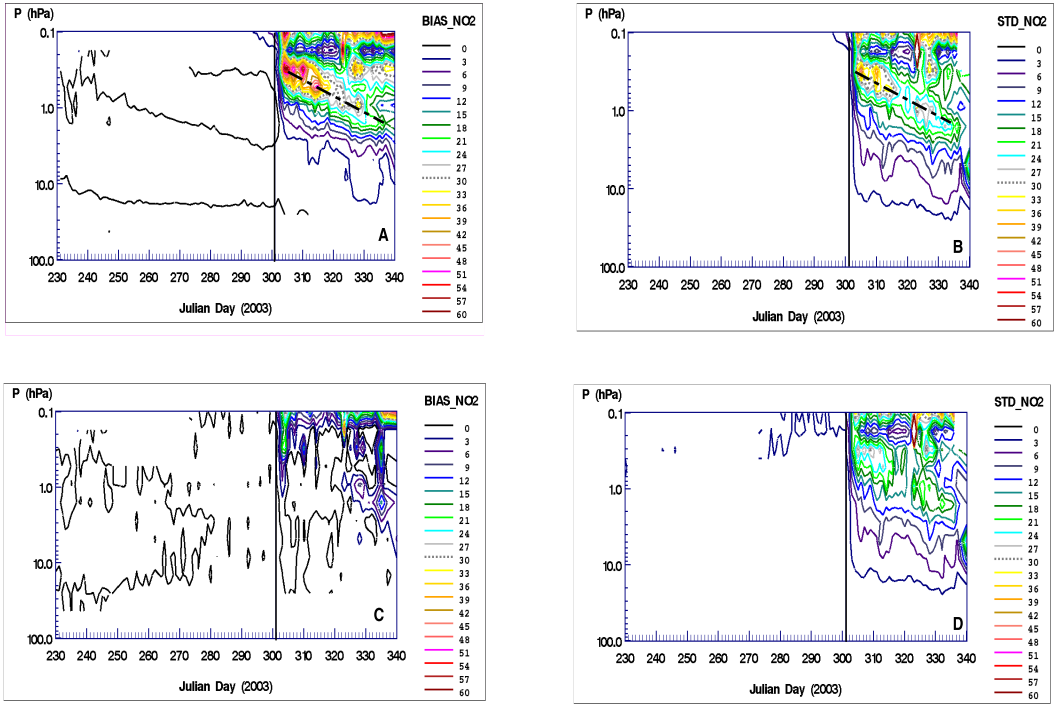

Fig. 7. Pressure-time plots of NO_2 *OmF* in ppbv for the SPE case (Halloween storm). Top panels: no chemical assimilation, **(A)** biases, **(B)** std. dev. Bottom panels: **(C)** and **(D)** are identical to (A) and (B) respectively but with chemical assimilation included. The domain is the North Pole (lat>60 N). The thin vertical line indicates the beginning of the SPE storm (28 Ocober 2003, i.e. Julian day 301). The dashed line represents the rate of descent of *OmF*.

ACPD
9, 22459–22504, 2009

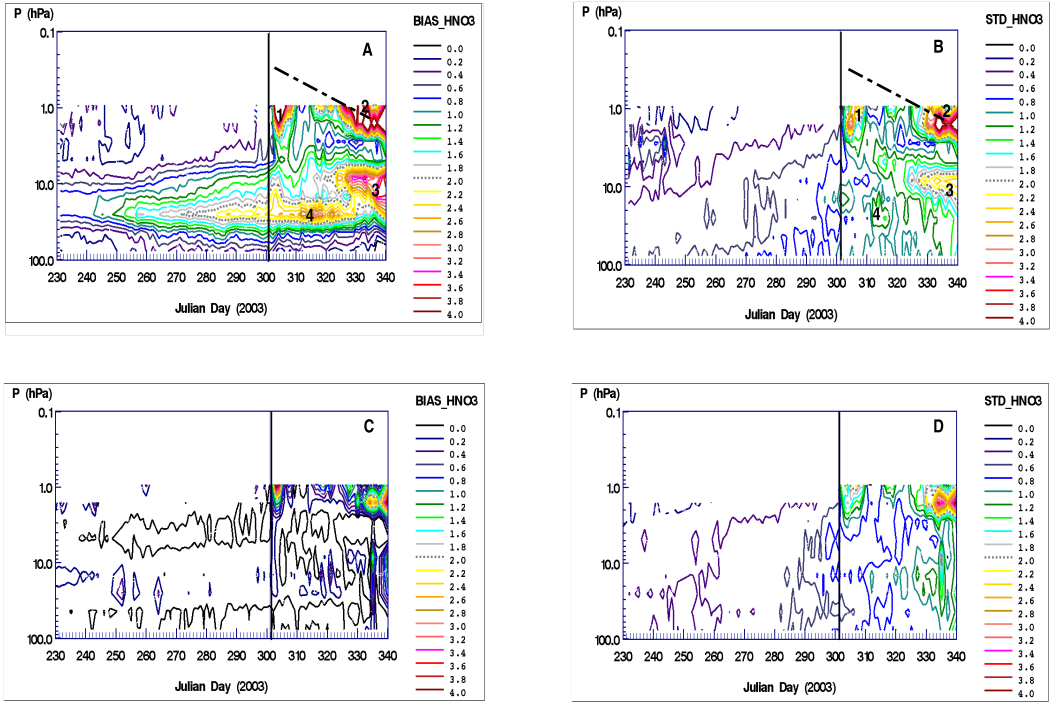

Fig. 8. As Fig. 7 but for HNO_3. The rate of descent for NO_2 *OmF* (dashed line) has been superimposed for reference purposes. No data is available for HNO_3 above roughly 1 hPa.

ACPD
9, 22459–22504, 2009

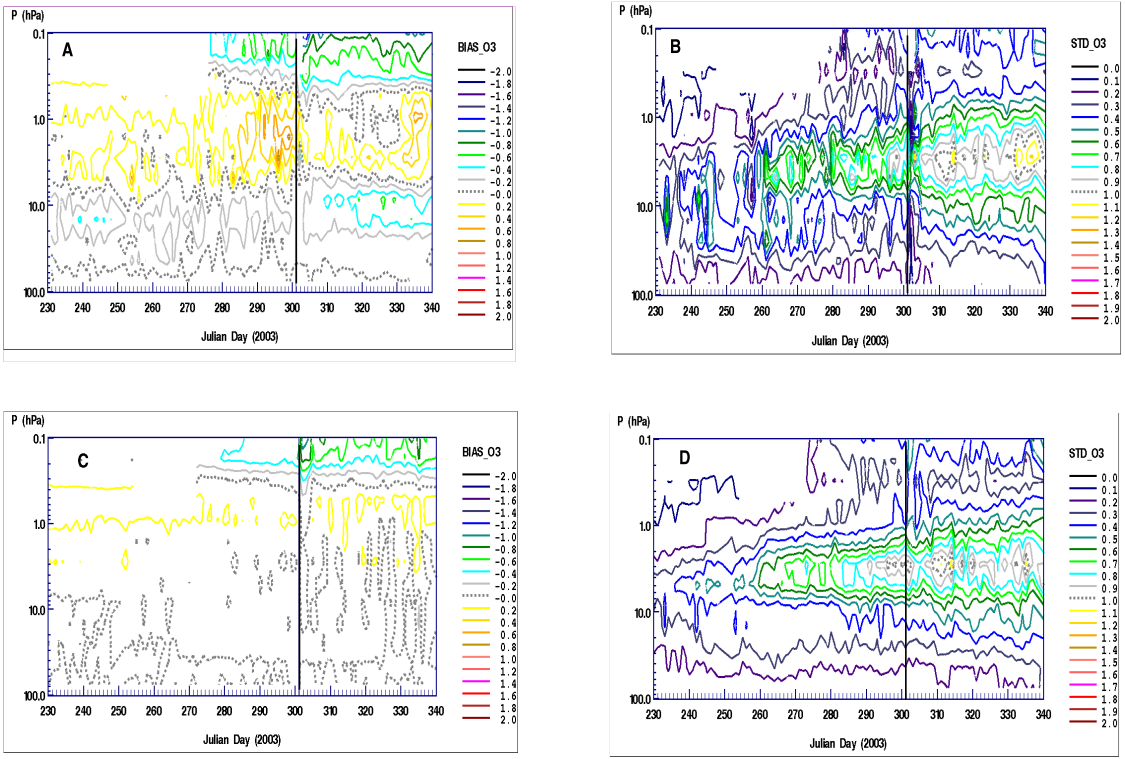

Fig. 9. As Fig. 8 but for O_3 (units are ppmv).

ACPD

9, 22459–22504, 2009

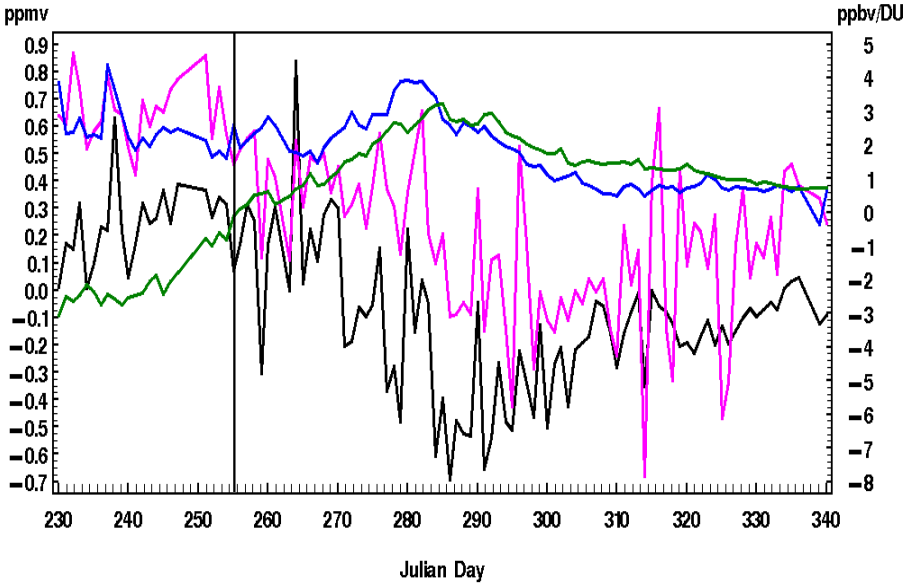

Fig. 10. Time series of passive *OmF* for O_3 (black), HNO_3 (green), and NO_2 (blue) at 14.5 hPa for the South Pole region (latitudes >60° S). Units are ppmv for O_3 and ppbv for HNO_3 and NO_2. The partial ozone column for *OmF* (in DU) is plotted in magenta. The vertical line roughly indicates the end of the polar night.

ACPD
9, 22459–22504, 2009

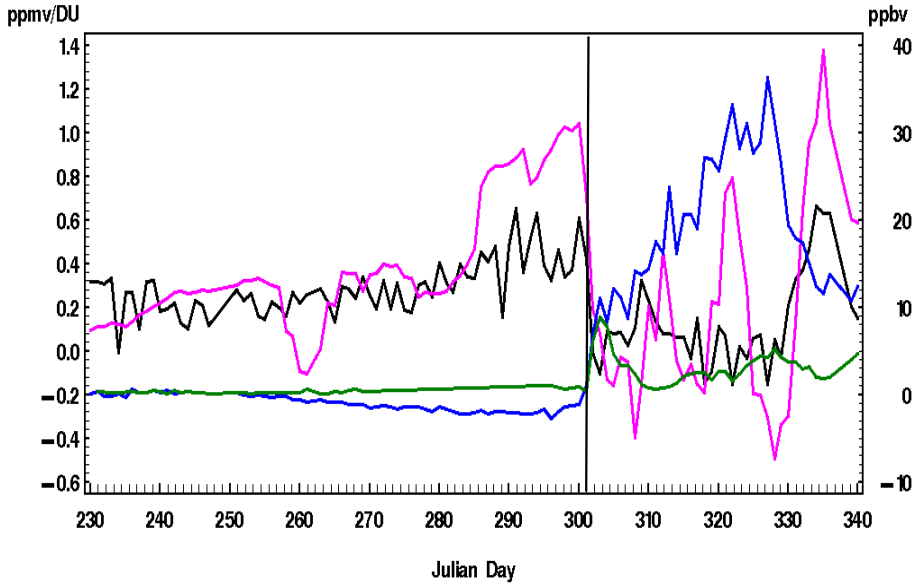

Fig. 11. Same as Fig. 10 but for the SPE case and centered at 1585 hPa in the North Pole region (latitude >60° N). The vertical line roughly indicates the onset of the impact of the SPE on the stratosphere (i.e. day 301).

ACPD
9, 22459–22504, 2009